# Use of phase angle in alternating voltammetry on redox self-assembled monolayers with intermolecular interactions

Olivier Alévêque, Eric Levillain

Graphical Abstract

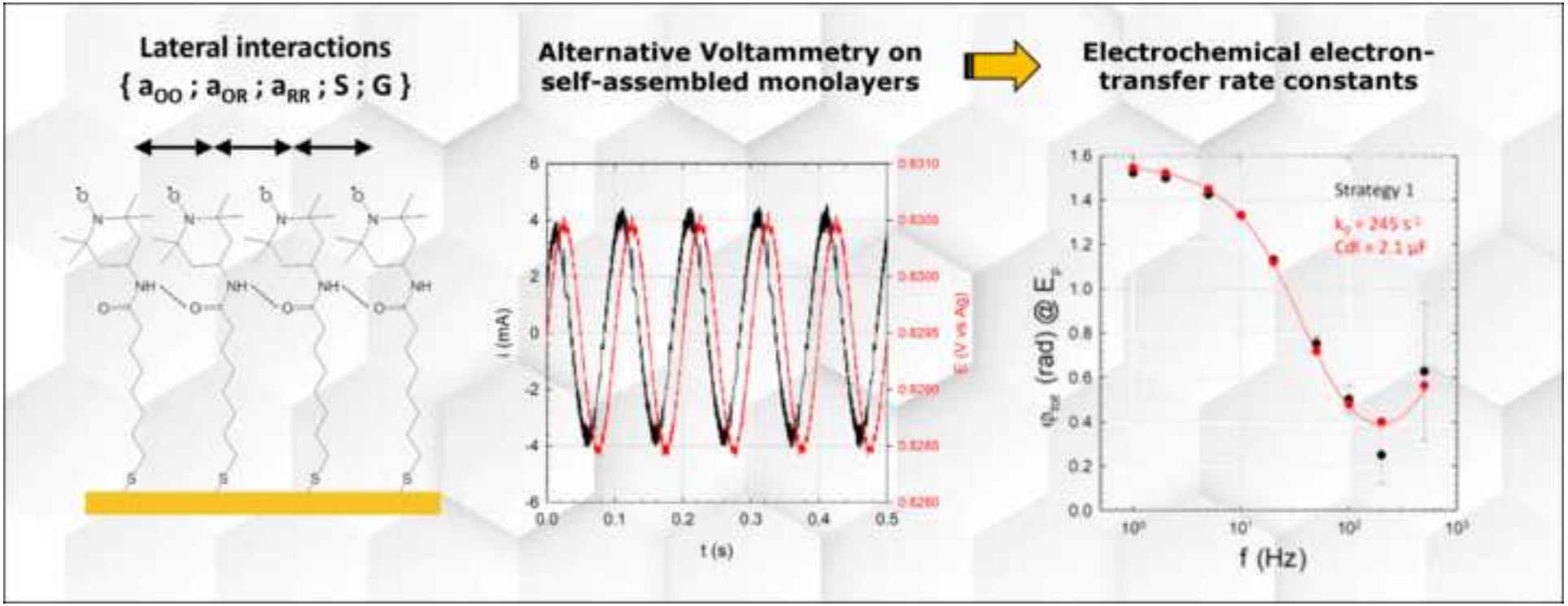

# Use of phase angle in alternating voltammetry on redox self-assembled monolayers with intermolecular interactions

Olivier Alévêque*, Eric Levillain

Université d'Angers, CNRS UMR 6200, Laboratoire MOLTECH-Anjou, SFR MATRIX, 2 boulevard Lavoisier, 49045, Angers Cedex, France

* Corresponding authors:
Olivier ALEVEQUE
Tel.: (+33)241735090
E-mail address: olivier.aleveque@univ-angers.fr

# FIGURES

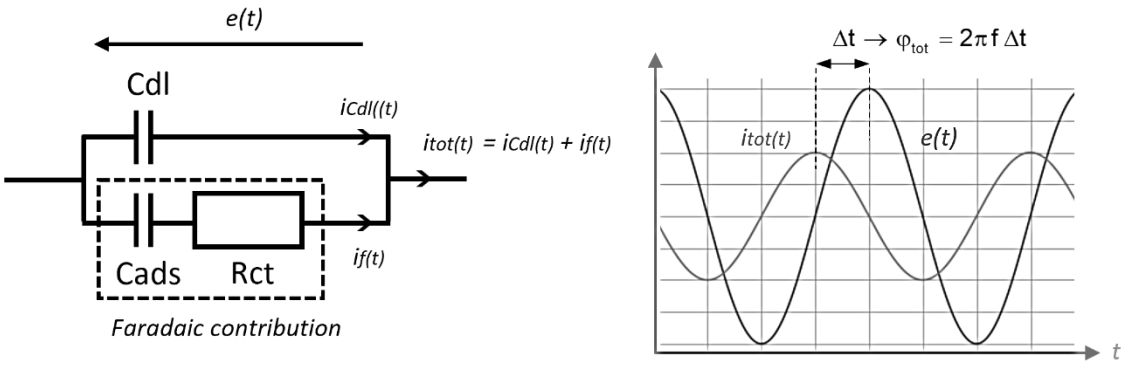


Figure 1: (**left**) Randles equivalent circuit for modelling a redox-active monolayer immobilized on electrode surface. Total current ($i_{tot}$) is composed of a faradaic ($i_f$) and a double layer ($i_{Cdl}$) current contributions. (**right**) Phase angle definition between the input voltage e(t) and resulting current $i_{tot}(t)$.

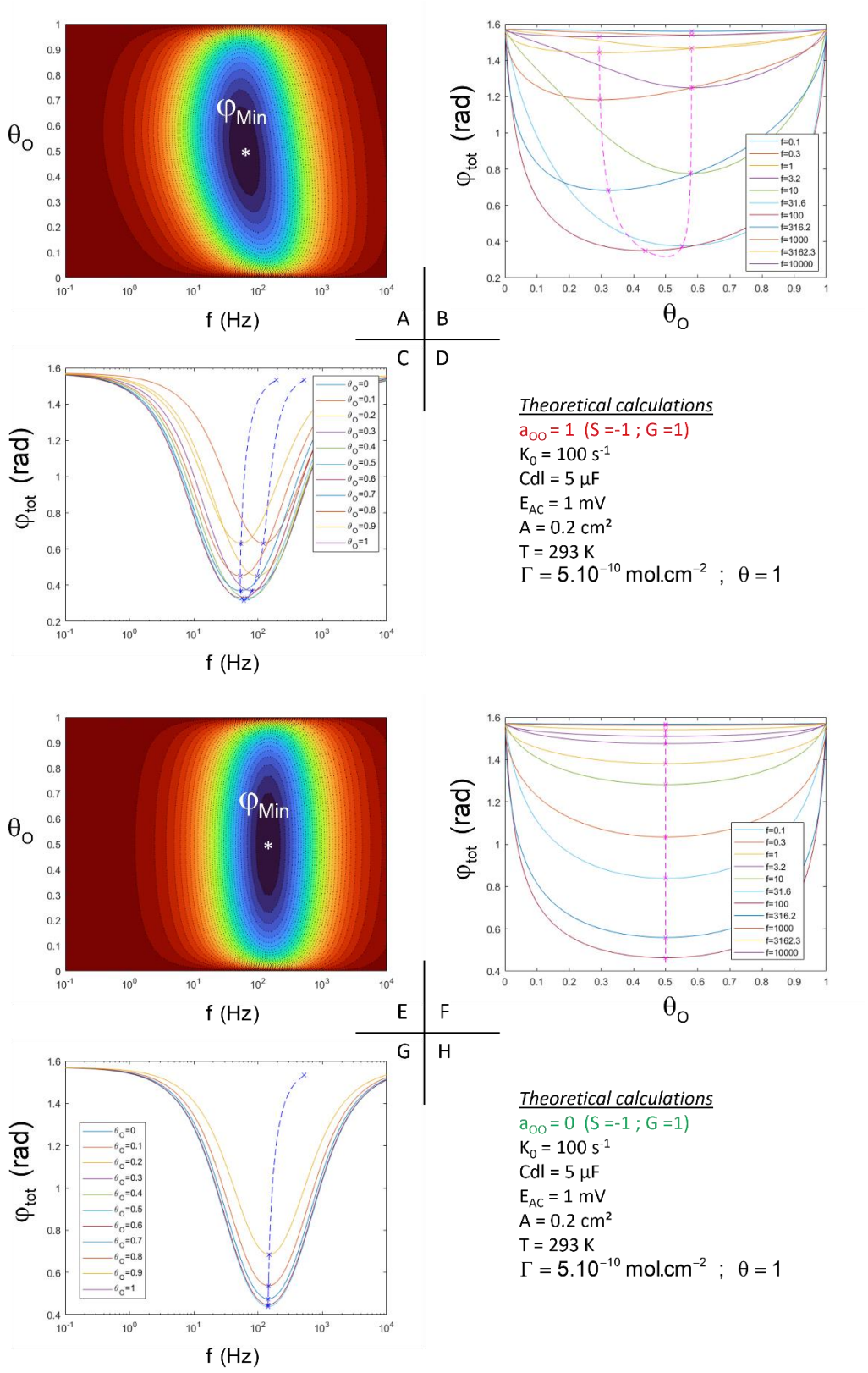


Figure 2: (**A**, **E**) 3D representation of $\varphi_{tot}$ vs. {$\theta_O$ and frequency} calculated from equation 14 for parameters listed in (**D**, **H**) respectively. (**B**, **F**) Stacked representations vs $\theta_O$ , with (x) local ON minima and (---) their trends. (**C**, **G**) Stacked representations vs frequency, with (x) local ON* minima and (---) their trends.

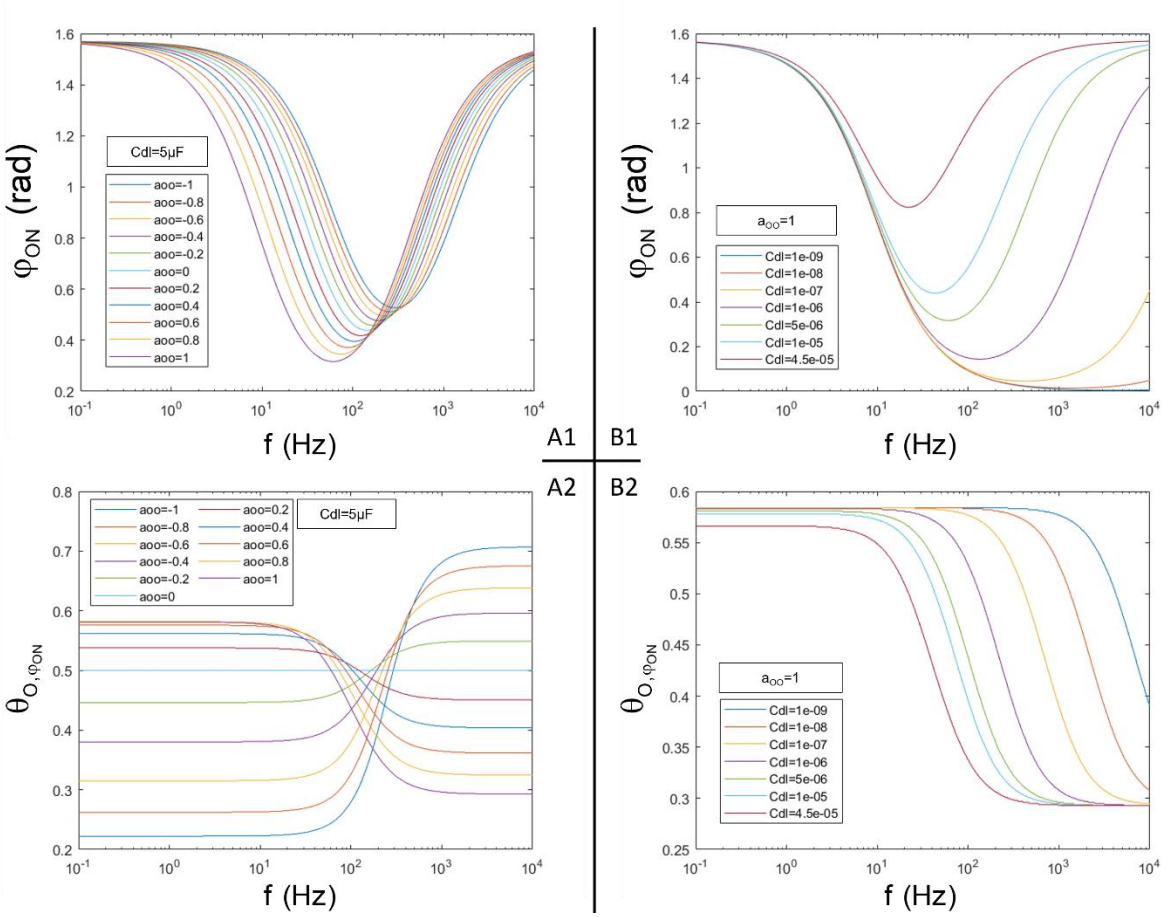


Figure 3: Evolution of the ON state location $\left\{\theta_{O,\varphi_{ON}}\ ;\ \varphi_{ON}\right\}$ vs frequency as a function of (**A1** and **A2**) interaction parameter ($a_{OO}$) or (**B1** and **B2**) Cdl. Used simulation parameters: $k_0$=100 $s^{-1}$, $E_{AC}$=1 mV, A=0.2 $cm^2$, T=293 K, Γ = $5.10^{-10}$ $mol.cm^{-2}$ (θ = 1).

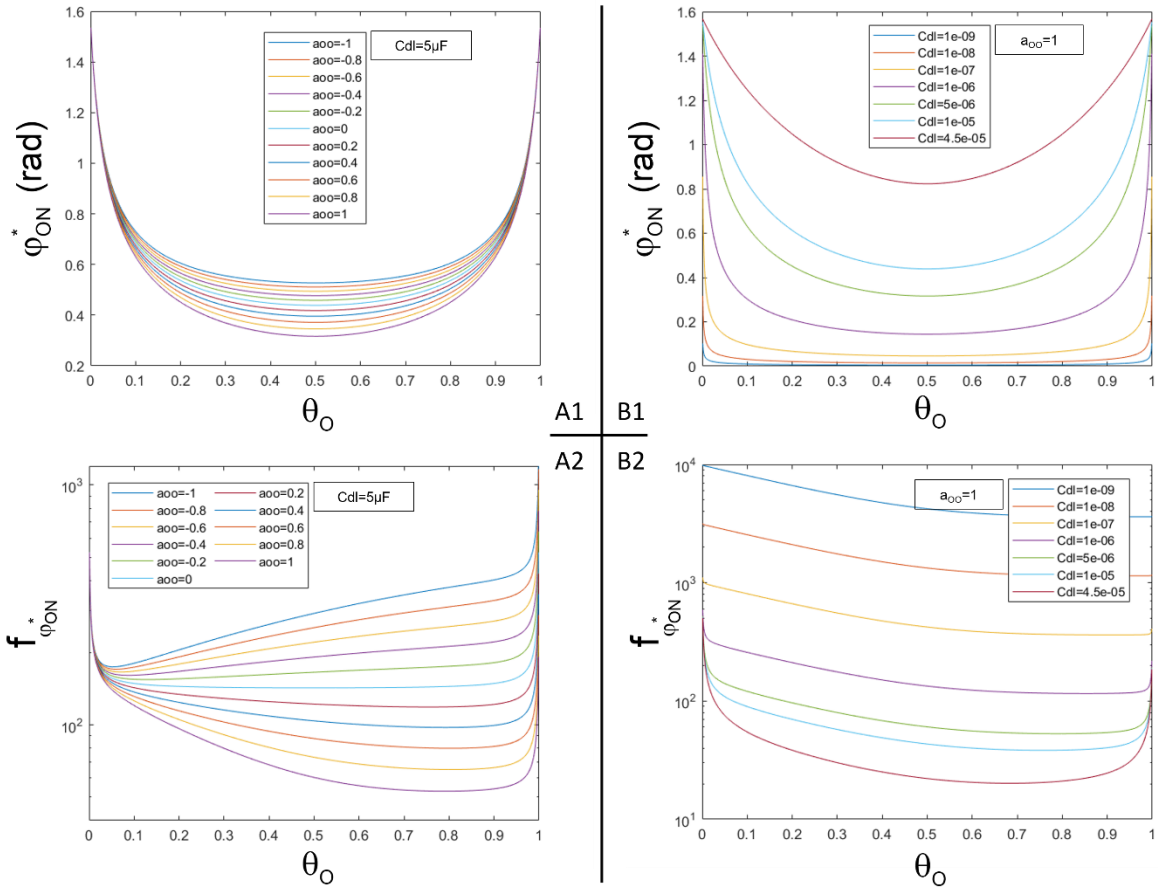


Figure 4: Evolution of the ON* state location $\left\{f_{\varphi_{ON}^*}; \varphi_{ON}^*\right\}$ vs $\theta_O$ as a function of (**A1** and **A2**) interaction parameter ($a_{OO}$) or (**B1** and **B2**) Cdl. Used simulation parameters: $k_0$=100 $s^{-1}$, $E_{AC}$=1 mV, A=0.2 $cm^2$, T=293 K, Γ = $5.10^{-10}$ $mol.cm^{-2}$ (θ = 1).

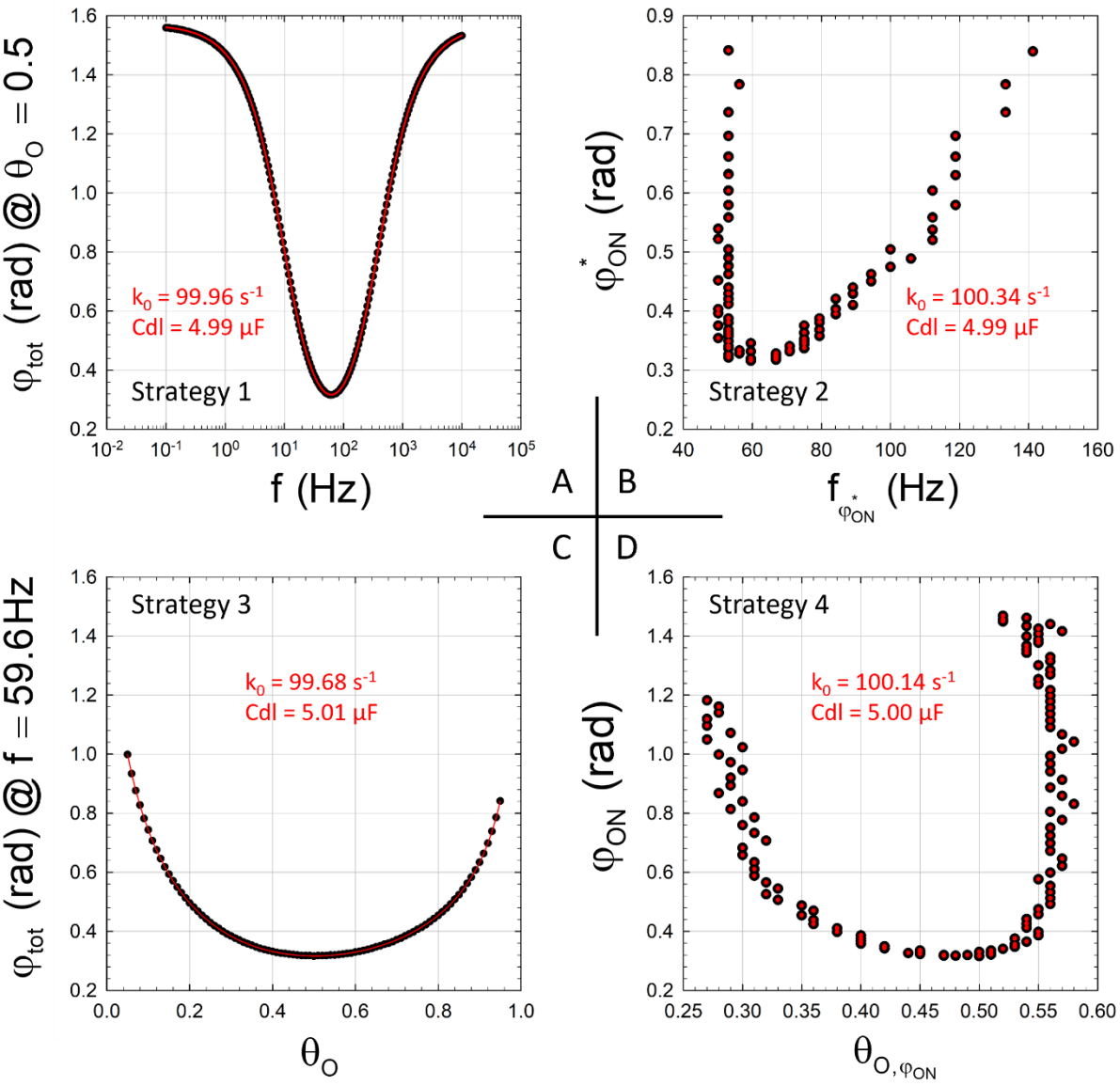


Figure 5: Fitting procedures applied to simulated AV generated at different frequencies and $\theta_O$ via the procedure described in § 2.2 with the following parameters: $k_0$=100 $s^{-1}$, Cdl = 5 µF, $a_{OO}$ = 1, α = 0.5, $E_{AC}$=1 mV, A=0.2 $cm^2$, T=293 K, Γ = 5.$10^{-10}$ mol.$cm^{-2}$ (θ = 1). (●) represents extracted values from AV and (● or -) the best estimated values. For each strategy, the best estimated parameters are:

(**A**) $k_0$ = 99.957 $s^{-1}$ ; σ($k_0$)= 0.034 $s^{-1}$ and Cdl = 4.9941 µF ; σ(Cdl) = 0.0022 µF

(**B**) $k_0$ = 100.34 $s^{-1}$ ; σ($k_0$)= 0.50 $s^{-1}$ and Cdl = 4.9871 µF ; σ(Cdl) = 0.0019 µF

(**C**) $k_0$ = 99.681 $s^{-1}$ ; σ($k_0$)= 0.046 $s^{-1}$ and Cdl = 5.0061 µF ; σ(Cdl) = 0.0016 µF

(**D**) $k_0$ = 100.137 $s^{-1}$ ; σ($k_0$)= 0.014 $s^{-1}$ and Cdl = 4.99611 µF ; σ(Cdl) = 0.00092 µF

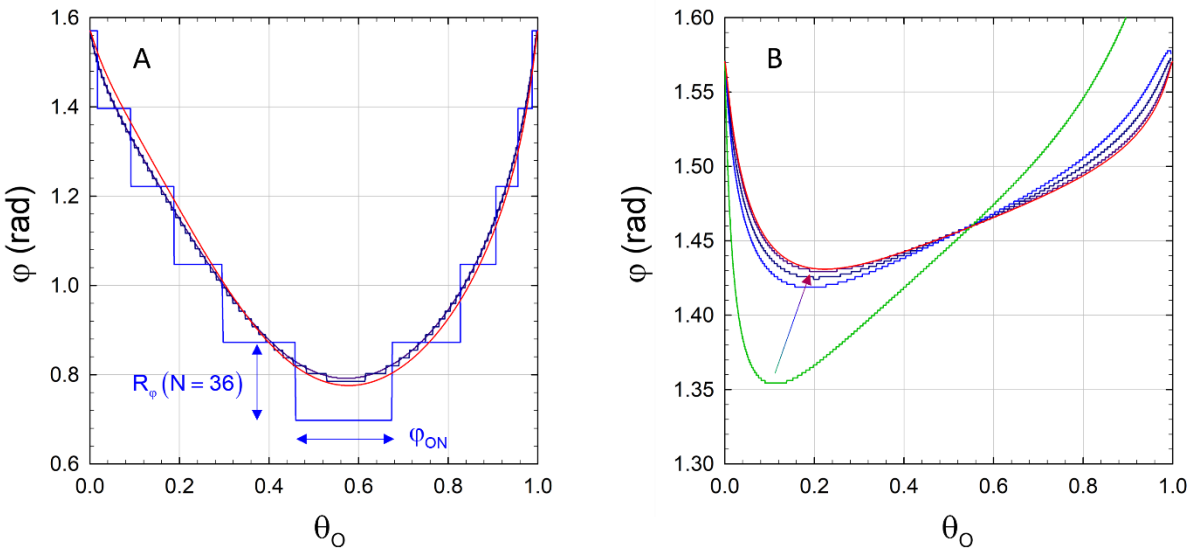


Figure 6: Dependence of the phase angle extracted from simulated AV with (**A**) the number of points per cycle N and (**B**) the potential amplitude $E_{AC}$. AV were generated via the procedure described in § 2.2 with the following parameters: $k_0$=100 $s^{-1}$, f = 10 Hz, Cdl = 5 µF, $a_{OO}$ = 1, α = 0.5, A=0.2 $cm^2$, T=293 K, Γ = $5.10^{-10}$ $mol.cm^{-2}$ (θ = 1) and (**A**) $E_{AC}$=0.001 mV, N=36 (blue), 360 (dark blue), 3600 (purple), theoretical (red) or (**B**) N=3600, $E_{AC}$=0.005 mV (green), 0.001 mV (blue), 0.0005 mV (dark blue), 0.0001 mV (purple), theoretical (red).

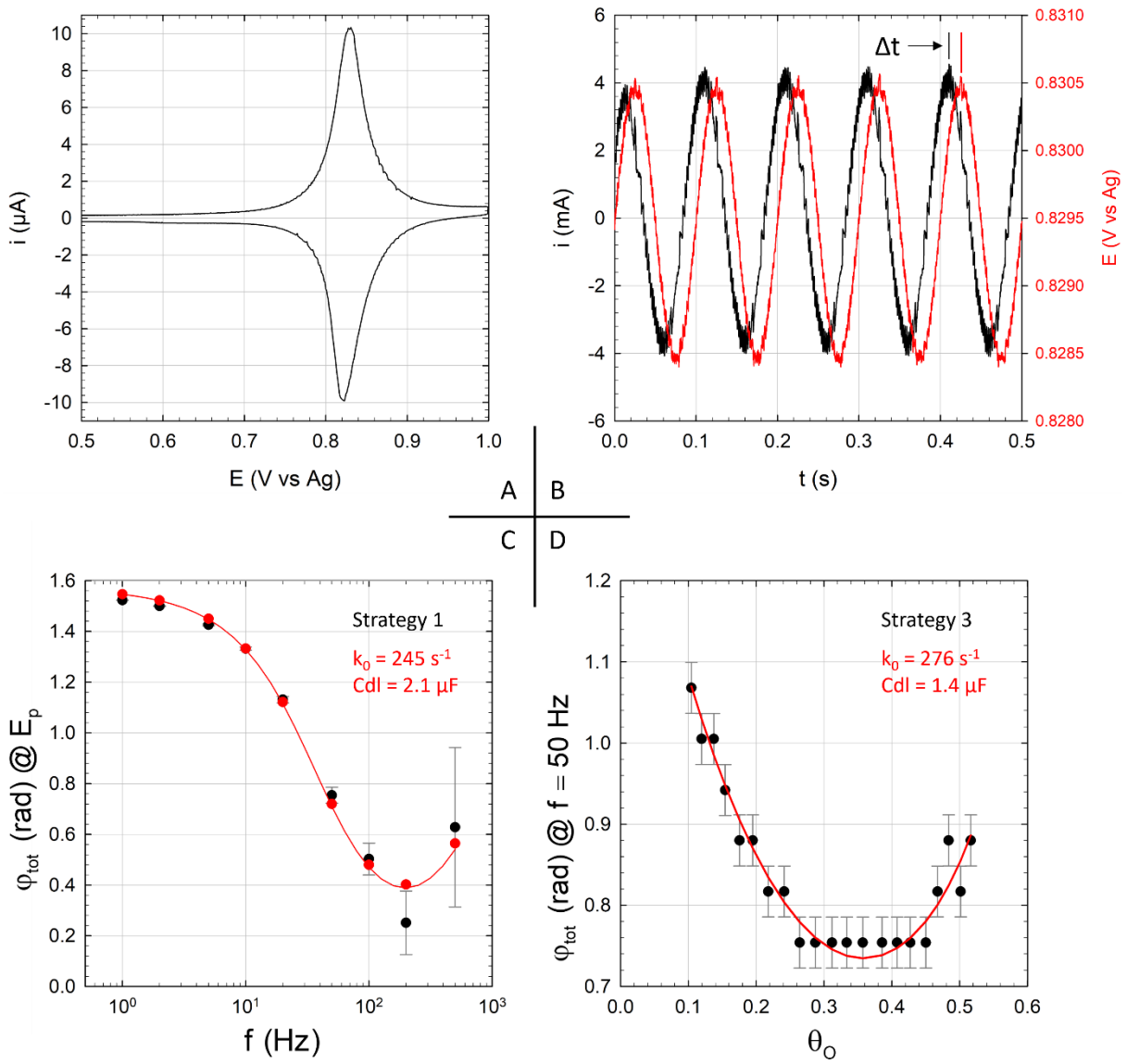


Figure 7: **A**) Experimental CV of C15-T self-assembled monolayer ($\Gamma = 3.1.10^{-10}$ mol.cm$^{-2}$ ($\theta = 0.62$), $a_{OO} = 1$) in 0.1 M $Bu_4NPF_6/CH_2Cl_2$ at 293 K and at v = 100 mV.s$^{-1}$ ($E_p$ = 0.829 mV vs Ag). **B**) Experimental AV of the SAM at the peak potential ($E_p$) (f = 10 Hz, $E_{AC}$ = 1 mV, $\Delta t_{acq}$ = 0.5 ms). **C**) $\varphi_{tot}$ obtained at the peak potential ($E_p$ ; $\theta_O = \theta / 2$) for each tested frequencies and **D**) $\varphi_{tot}$ obtained at 50 Hz for each tested $\theta_O$ (potential E converted into $\theta_O$ via GLI function). (●) represents extracted values from AV and (● or -) the best estimated values. For each strategy, the best estimated parameters are: (strategy 1) $k_0$ = 245 s$^{-1}$ ; $\sigma(k_0)$= 22 s$^{-1}$ and Cdl = 2.10 µF ; $\sigma$(Cdl) = 0.31 µF and (strategy 2) $k_0$ = 276 s$^{-1}$ ; $\sigma(k_0)$= 17 s$^{-1}$ and Cdl = 1.4 µF ; $\sigma$(Cdl) = 1.8 µF

# Use of phase angle in alternating voltammetry on redox self-assembled monolayers with intermolecular interactions

Olivier Alévêque*, Eric Levillain

Université d'Angers, CNRS UMR 6200, Laboratoire MOLTECH-Anjou, SFR MATRIX, 2 boulevard Lavoisier, 49045, Angers Cedex, France

* Corresponding authors:
Olivier ALEVEQUE
Tel.: (+33)241735090
E-mail address: olivier.aleveque@univ-angers.fr

**ARTICLE INFO**

**Keywords:**

Alternative Voltammetry
Lateral interactions
Electroactive self-assembled monolayers
Electrochemical simulations
Electrochemical fitting

**ABSTRACT**

We present a methodology based on the study of the frequency dependence of the phase angle in Alternative Voltammetry to estimate the standard electrochemical rate constant for heterogeneous electron transfer reactions in the case of strong intermolecular interactions occur between the redox forms.
This work is a follow-up to our previous study which was dedicated only to the study of peak currents.

## 1. Introduction

Heterogeneous electrochemical processes on redox-responsive materials (i.e., conductive polymers, multilayer, thin films and self-assembled monolayers) are known to play a key role in fields such as electrochemical sensors, electrocatalysis-based devices, electrochemical synthesis, molecular electronics and the reliable estimation of the electrochemical rate constant has become, among other parameters, a challenge to understand the interfacial electrochemical mechanisms involved.
In this context, since their discovery[1], self-assembled monolayers (SAMs) have become an ideal system for studying interfacial phenomena as closely as possible to proposed theories, thanks to their simplicity of preparation, their relatively good stability, and the possibility of modulating all the parts of the grafted molecule (anchoring group, spacer, functional group, etc.) in order to modify the properties studied[2].
To provide relevant information on electrochemical processes involved, many models and theories have been developed[3,4] and studied specifically by more or less complex electrochemical techniques (cyclic voltammetry[5–7], impedance spectroscopy[8], square-wave voltammetry[9,10], square-wave voltcoulometry[11], chronoamperometry[12,13], small-amplitude alternative voltammetry (AV)[14–17], large-amplitude alternative voltammetry[18–21] …). Some of them have made it possible to model systems in which strong intermolecular interactions occur between the redox forms[22].

Cyclic voltammetry (CV) is known to be the most frequently used electrochemical technique to achieve this objective because, based on Laviron's model, the standard electrochemical rate constant ($k_0$) can be deduced from the shift of the peak potentials as a function of the scan rate[23]. However, this method remains very random for high scan rates, which limits the determination of electrochemical rate constants to not too large values. In order to provide a new alternative approach, our previous paper[24] described two methods based on alternative cyclic voltammetry (ACV) technique to estimate the standard electrochemical rate constants ($k_0$) of immobilized redox molecules presenting intermolecular interactions and described by the general lateral interaction model initiated by Laviron[14] and update over time[25,26].
The theoretical part, in which the redox reaction is described by Butler-Volmer (BV) kinetic formalism under Nernstian conditions for the non-alternative component of the perturbating signal e(t), extends the Creager and Wooster's method[14] and allowed to define the expression of the ratio $I_{ON}/I_{OFF}$ during an ACV experiment. In this work, we deal with the same problematic using the second important parameter of an AC signal, namely the phase angle. Even if this approach is difficult to implement with current technologies, the first results obtained are quite encouraging.

## 2. Experimental conditions

### 2.1 Reagents, chemical and preparation of SAMs at gold electrodes

The relevance of our approaches was tested via TEMPO-based self-assembled monolayers (C15-TEMPO) on Au substrate, known to provide very intense attractive interactions between its oxidized species in methylene chloride. The synthesis, characterisations and preparation of C15-TEMPO were described in Ref[27].

### 2.2. Electrochemical measurements

Electrochemical experiments were carried out with a Biologic SP-300 potentiostat driven by the EC-Lab software including ohmic drop compensation. All electrochemical experiments were performed in a three-electrode cell controlled at a temperature of 293 K in a glove box containing dry, oxygen-free (< 1 ppm) argon. Working electrodes were a gold modified surface. Counter electrodes were platinum wires. Reference electrodes were Ag wire or $Ag/AgNO_3$ (0.01 M $CH_3CN$) in order to have a very fine determination of the potential. Experiments were recorded in dry HPLC-grade methylene chloride with tetrabutylammonium hexafluorophosphate ($Bu_4NPF_6$, electrochemical grade, Fluka) as supporting electrolyte.

All the procedures described in the following sections must be performed in a defined order: studies of the SAMS by 1) cyclic voltammetry to reduce the number of unknows, follow by 2) alternative voltammetry. Table 1 lists symbols used hereinafter.

#### Cyclic voltammograms

Cyclic voltammograms (CV) were essentially performed under Nernstian conditions (scan rate $v << k_0$) to allow the extraction of the full width at half maximum (FWHM), peak potential (Ep) and peak intensity (ip). Interactions which influence these parameters can thus be estimated. In addition, Cdl can be roughly estimated by dividing the capacitive current by the scan rate $\left(Cdl = i_{cap} / v\right)$. The charge (Q) involved during a CV experiment is

deduced by integration of the voltammetric signal, and the surface coverage of electroactive species is calculated as $\Gamma = Q/(nFA)$ with A the area of the electrode, F the faraday constant and n the number of electrons involved during the process.

**Alternatives voltammograms**

Alternative voltammetry (AV) experiments on the same SAMs were performed with a small amplitude voltage of 1-5 mV ($E_{AC}$), a scan rate (v) of 1-5 mV.s$^{-1}$ for ACV, and an acquisition time adjusted to obtain at least 36 points per alternative cycle whatever the frequency (f) used. Generally, at least five frequencies per decade were used between 1 mHZ and 500 Hz (*i.e.,* the maximum frequency of our instrument) to obtain the minimum number of points needed to perform the proposed adjustment procedures. Ohmic drop compensation should be used to compensate for the resistance of the electrolytic solution as accurately as possible.

**Generation of simulated voltammograms**

As previously described[24], all simulated cyclic voltammograms (CV), alternative voltammograms (AV) and alternative cyclic voltammograms (ACV) were performed using SigmaPlot 14.5 and/or MATLAB R2020b softwares run on a conventional desktop computer (Intel Core i7-10810U CPU @ 1.10GHz 6 cores). We used a simple numerical method approximating the continuous variation of the applied potential as a series of potential steps ΔE. With an increment ΔE small enough, it is possible to assume that the oxidation ($k_b$) and reduction ($k_r$) rate constants are quasi constant during the step. This procedure is detailed in previous papers[28] and adapted to our formalism.

In the case of a reversible n-electron process of adsorbed electroactive species following the general lateral interaction model (*vide infra*), CV, AV or ACV voltammograms can be simulated with this set of equations:

$$O + ne^- \underset{kb}{\overset{kf}{\rightleftharpoons}} R$$

$$i = nFA\Gamma_{max}\frac{d\theta_O}{dt} = nFA\Gamma_{max}\left(k_b\left(\theta-\theta_O\right)-k_f\,\theta_O\right)$$

$$\theta_O(i+1) = \left(\theta_O(i) - \frac{k_b(i+1)\,\theta}{k_b(i+1)+k_f(i+1)}\right)\exp\left(-\left(k_b(i+1)+k_f(i+1)\right)\Delta t\right) + \frac{k_b(i+1)\,\theta}{k_b(i+1)+k_f(i+1)}$$

$$\Delta\theta_O = \theta_O(i+1)-\theta_O(i) = \left(\frac{k_b(i+1)\,\theta}{k_b(i+1)+k_f(i+1)}-\theta_O(i)\right)\left(1-\exp\left(-\left(k_b(i+1)+k_f(i+1)\right)\Delta t\right)\right)$$

with
$$\begin{cases} \theta_O(j)\ \text{the value of}\ \theta_O\ \text{at step j} \\ k_b(i+1) = k_0\exp\left((1-\alpha)\frac{nF}{RT}\left(E(i+1)-E^{0'}\right)\right)\exp\left(-2a_{RR}\frac{\phi(\theta)}{\theta}\theta_R(i)-2a_{OR}\frac{\phi(\theta)}{\theta}\theta_O(i)\right) \\ k_f(i+1) = k_0\exp\left(-\alpha\frac{nF}{RT}\left(E(i+1)-E^{0'}\right)\right)\exp\left(-2a_{OO}\frac{\phi(\theta)}{\theta}\theta_O(i)-2a_{OR}\frac{\phi(\theta)}{\theta}\theta_R(i)\right) \\ E(i+1) = \left(E_i+vt\right)+E_{AC}\sin(wt) = \left(E_i+(i+1)\,\Delta t\,v\right)+E_{AC}\sin\left((i+1)\Delta t\,w\right) \end{cases}$$

## 3. Theoretical prerequisites on the models and formalisms used

### 3.1. The general lateral interaction model

The generalized lateral interaction model (GLI model) enables current-voltage behaviours (CV, ACV, …) to be simulated in the case of a reversible n-electron process of adsorbed electroactive species. It was updated to

include the effects of non-random distributions of electroactive species, interactions between redox and non-redox species and the possibility to use binary electrolyte mixture[29].

For ease of reading, here is a summary of the main hypotheses if we only select the case of interactions between redox species:

- Strongly adsorbed electroactive species are only oxidized and reduced at the adsorbed state.
- The electroactive species are theoretically grafted on the electrode according to a unimodal statistical distribution of the electroactive neighbours, with a spatial regularity (random or not). The surface occupied by an oxidized molecule, or a reduced molecule is the same.
- The segregation level of the electroactive species is quantified with a normalized parameter $\phi(\theta)$ ( $\theta < \phi(\theta) < 1$), defined for a normalized surface coverage $\theta = \frac{\Gamma}{\Gamma_{max}}$ $\begin{matrix}\leftarrow \text{surface coverage (mol.cm}^{-2}\text{)} \\ \leftarrow \text{saturated surface coverage (mol.cm}^{-2}\text{)}\end{matrix}$. For a randomly distributed SAM, $\phi(\theta) = \theta$.
- The sum of normalized surface coverage of oxidized and reduced species is equal to the normalized surface coverage: $\theta_O + \theta_R = \theta$.
- The standard electrochemical rate constant ($k_0$) at the heterogenous standard potential ($E^{0'}$) is considered as a constant.
- $a_{OO}$, $a_{RR}$ and $a_{OR}$ are the potential-independent interaction constants between molecules of O, molecules of R and molecules of O and R, respectively, and are positive for an attraction and negative for a repulsion.
- The influence of lateral interactions in the electro-chemical response of the surface redox probes is visualized through potential-independent global interaction parameters G and S, defined as $G = (a_{OO} + a_{RR} - 2a_{OR})$ , $S = (a_{RR} - a_{OO})$ with G ≤ 2. Overall, $G \cdot \phi(\theta)$ changes the shape of the voltametric peak, *i.e.,* the FWHM and the peak intensity, whereas $S \cdot \phi(\theta)$ controls the position of the peak potential. During a CV experiment under Nernstian conditions ($k_0$ >> v), these parameters are defined as:

$$\begin{cases} E_p(\theta) = E^{0'} + \dfrac{R\,T}{nF} S\,\phi(\theta) \\ I_p(\theta) = \dfrac{n^2F^2vA\Gamma_{max}}{2RT} \dfrac{\theta}{(2 - G\,\phi(\theta))} \\ FWHM(\theta) \overset{|G\phi(\theta)|<1}{\approx} \dfrac{R\,T}{nF}\left[2\ln(2\sqrt{2}+3) - \dfrac{3\sqrt{2}}{2} G\,\phi(\theta)\right] \end{cases} \quad (1)$$

With n, F, A, R, T, E and v having their usual meanings and $E^{0'}$ the apparent standard surface potential.

### 3.2. General Lateral Interaction Function (GLI function)

Based on the General Lateral Interaction model, the GLI function has initially been developed to fit cyclic voltammetric peaks of SAMs under Nernstian conditions (v << $k_0$) to extract the main characteristic parameters as the peak current ($i_p$), the full width at half maximum (FWHM) and the peak potential ($E_p$).

This model[30] is defined according to an approximation of $\theta_O$ to work around a problem of mathematical recursion and leads to directly link the potential E to $\theta_O$.

$$\begin{cases} \theta_O = \dfrac{\theta}{1+\exp\left(-\dfrac{nF}{RT}\left(E-E_p\right)\lambda\right)} \quad \text{and} \quad E-E_{p\,CV} = -\dfrac{RT}{nF\lambda}\ln\left(\dfrac{\theta-\theta_O}{\theta_O}\right) \\ \text{with} \quad \lambda = 1/\left(1-0.399\cdot G\cdot\phi(\theta)\right) \overset{\text{randomly distributed SAM}}{\Rightarrow} \lambda = 1/\left(1-0.399\cdot G\cdot\theta\right) \end{cases} \tag{2}$$

### 3.3. Alternative (Cycling) Voltammetry characteristics

AV involves the application of a sinusoidal voltage combined with voltage sweep at a scan rate v ($V.s^{-1}$) to a modified electrode surface. When v=0, it is about AV.

$$\begin{cases} \text{ACV} & e(t) = E(t) + E_{AC}\sin(wt) = \left(E_i + v\cdot t\right) + E_{AC}\sin(wt) \quad \text{with} \quad w = 2\pi f \\ \text{AV} & e(t) = E_{DC} + E_{AC}\sin(wt) \end{cases} \tag{3}$$

A differentiation is made according to the amplitude of the sinusoidal part: if $E_{AC}$ is high enough the technique is called Large Amplitude AV and conversely when $E_{AC}$ is small in comparison to the global change in voltage the technique is called Small Amplitude AV.

Here, small amplitude Alternative Cyclic Voltammetry is used under two major conditions:

1. The variation of the surface concentration of redox species must be small at each cycle to obtain a sinusoidal resulting current [3]. In this case, mathematical treatments based on equivalent circuits can be used, taking advantage of the linearization of the kinetics of the electrodes, which initially have an exponential dependence on the applied voltage. Typically, a small amplitude of 5 mV or less is chosen depending on the interactions, especially when the interactions produce a fast surface concentration variation of the redox state of electroactive species close to apparent standard potential.
2. Scan rate (v) must be lower than $k_0$ in order to respect the Nernst conditions (DC component only considered) and, also, to have an AC current higher than the DC current (i.e. conditions similar to a multitude of AV at different potential).

### 3.4. The formalism used for Alternative (Cyclic) Voltammetry

From the above experimental conditions of AV, redox SAMs can be modelled with the Randles equivalent circuit (figure 1).

Depending on the potential applied, the Randles equivalent circuit presents two boundary simplifications:

1. When the faradaic contribution is negligible, far away from the apparent standard potential, the resulting current is only due to the double layer capacitance contribution. This case is denominated as OFF state:

$$i_{Cdl} = I_{Cdl}\sin\left(wt+\varphi_{Cdl}\right) \quad \Leftrightarrow \quad i_{OFF} = I_{OFF}\sin\left(wt+\varphi_{OFF}\right) \tag{4a}$$

2. When the faradaic contribution is not negligible (named here “tot” for total state), the resulting current is the sum of faradaic and double layer capacitance contributions.

   At a given frequency, two peculiars ON states co-exist at specified potentials (or $\theta_O$) when the current magnitude is maximum ($I_{ON}$) and when the phase angle passes through a minimum ($\varphi_{ON}$). We emphasize on this coexistence because these two cases may or may not occur at the same potential.

$$i_{tot} = i_{Cdl} + i_f = I_{tot}\sin\left(wt + \varphi_{tot}\right) \overset{\text{ON States at fixed frequencies}}{\Rightarrow} \begin{cases} i_{tot} = i_{I_{ON}} = I_{ON}\sin\left(wt + \varphi_{I_{ON}}\right) & \text{at } \theta_{O,I_{ON}} \\ i_{tot} = i_{\varphi_{ON}} = I_{\varphi_{ON}}\sin\left(wt + \varphi_{ON}\right) & \text{at } \theta_{O,\varphi_{ON}} \end{cases} \quad (4b)$$

   At a given potential (or $\theta_O$), another ON* state exists when the phase angle reaches a minimum ($\varphi^*_{ON}$) at a specified frequency ($w_{\varphi^*_{ON}}$):

$$i_{tot} = i_{Cdl} + i_f = I_{tot}\sin\left(wt + \varphi_{tot}\right) \overset{\text{ON* State at fixed potentials}}{\Rightarrow} \left\{ i_{tot} = i_{\varphi^*_{ON}} = I_{\varphi^*_{ON}}\sin\left(w_{\varphi^*_{ON}}\, t + \varphi^*_{ON}\right) \right. \quad (4c)$$

   Note that, if the applied potential is constant, the $I_{ON}$* states do not exist, $I_{tot}$ increasing continuously with frequency.

From the formalism devoted to AC polarograms in the case of strongly adsorbed and randomly distributed electroactive species [4–6], Rct and Cads can be explicit by equation 5:

$$\begin{cases} Rct = \dfrac{RT}{n^2F^2A\Gamma_{max}}\dfrac{1}{k_0\,\chi} \\ \dfrac{1}{Cads} = \dfrac{RT}{n^2F^2A\Gamma_{max}}\dfrac{\xi}{\chi} \end{cases} \Rightarrow \; ko\,\xi = \frac{1}{Rct\,Cads} \quad (5)$$

with

$$\begin{cases} \chi = (1-\alpha)\theta_R\eta^{1-\alpha}e^{-2a_{RR}\theta_R - 2a_{OR}\theta_O} + \alpha\theta_O\eta^{-\alpha}e^{-2a_{OO}\theta_O - 2a_{OR}\theta_R} \\ \xi = \left(1 + 2\left(a_{OR} - a_{RR}\right)\theta_R\right)\eta^{1-\alpha}e^{-2a_{RR}\theta_R - 2a_{OR}\theta_O} + \left(1 + 2\left(a_{OR} - a_{OO}\right)\theta_O\right)\eta^{-\alpha}e^{-2a_{OO}\theta_O - 2a_{OR}\theta_R} \end{cases} \quad (6)$$

At the equilibrium potential (*i.e.,* in small amplitude ACV experiment when $v \ll k_0$), $\eta$ can be expressed following:

$$\eta = e^{\frac{nF}{RT}\left(E - E^{0'}\right)} = \frac{\theta_O}{\theta_R}e^{2\theta_O\left(a_{OR} - a_{OO}\right) + 2\theta_R\left(a_{RR} - a_{OR}\right)} = \frac{\theta_O}{\theta - \theta_O}e^{-2G\theta_O + \theta(S+G)} \quad (7)$$

with $\theta_O$ and $\theta_R$ are the values in the absence of alternative potential at $E = E_i + v \cdot t$.

With simplifying assumptions such as a charge transfer coefficient ($\alpha = 0.5$) and a randomly distributed SAM (i.e. $\phi(\theta) = \theta$), equation 6 becomes:

$$\begin{cases} \chi = \sqrt{\theta_O\theta_R}\,e^{-\theta_O\left(a_{OO} + a_{OR}\right) - \theta_R\left(a_{RR} + a_{OR}\right)} = \sqrt{\theta_O\left(\theta - \theta_O\right)}e^{\theta_O S - \theta\left(a_{RR} + a_{OR}\right)} \\ \xi = \chi\dfrac{\theta - 2G\theta_O\theta_R}{\theta_O\theta_R} = \chi\dfrac{\theta - 2G\theta_O\left(\theta - \theta_O\right)}{\theta_O\left(\theta - \theta_O\right)} \end{cases} \quad (8)$$

It must be emphasized that Rct and Cads are not constant but depend on the surface coverage of reduced and oxidized species (*i.e.,* the potential applied) and on the interaction parameters (G, S, $a_{ij}$).

The total resulting current defined according to the Randles equivalent circuit associated to the formalism above (equation 5) can be expressed as follows:

$$
\begin{cases}
i_{tot} = i_{Cdl} + i_f = I_{Cdl}\sin\left(wt + \varphi_{Cdl}\right) + I_f \sin\left(wt + \varphi_f\right) = I_{tot}\sin\left(wt + \varphi_{tot}\right) \\
\begin{cases} I_{Cdl} = w\,Cdl\,E_{AC} \quad \left(= I_{OFF}\right) \\ \varphi_{Cdl} = \dfrac{\pi}{2} \end{cases} \\
\begin{cases} I_f = \dfrac{E_{AC}}{\sqrt{Rct^2 + \left(\dfrac{1}{w\,Cads}\right)^2}} = \dfrac{\dfrac{n^2F^2A\Gamma_{max}}{RT}E_{AC}}{\sqrt{\left(\dfrac{1}{ko\,\chi}\right)^2 + \left(\dfrac{\xi}{w\,\chi}\right)^2}} \\ \varphi_f = \arctan\left(\dfrac{1}{w\,Rct\,Cads}\right) = \arctan\left(\dfrac{k_0\,\xi}{w}\right) \end{cases} \\
\begin{cases} I_{tot} = w\,Cdl E_{AC}\sqrt{\dfrac{Rct^2\,Cads^2\,w^2 + \left(\dfrac{Cads}{Cdl} + 1\right)^2}{1 + Rct^2\,Cads^2\,w^2}} = I_{OFF}\sqrt{\dfrac{Rct^2\,Cads^2\,w^2 + \left(\dfrac{Cads}{Cdl} + 1\right)^2}{1 + Rct^2\,Cads^2\,w^2}} \\ \varphi_{tot} = \arctan\left(\dfrac{Rct^2\,Cads^2\,Cdl\,w^2 + Cads + Cdl}{w\,Rct\,Cads^2}\right) \end{cases}
\end{cases}
\tag{9}
$$

$I_{tot}$ can expressed using two different mathematical approaches:

$$
I_{tot} = I_{OFF}\sqrt{\frac{\rho^2 + \left(\dfrac{w}{k_0\,\xi}\right)^2}{1 + \left(\dfrac{w}{k_0\,\xi}\right)^2}} \quad \text{with} \quad \rho = 1 + \frac{n^2F^2A\Gamma_{max}}{Cdl\,RT}\frac{\chi}{\xi} \tag{10a}
$$

or (Appendix A),

$$
I_{tot} = \sqrt{I_f^{\,2} + I_{Cdl}^{\,2} + 2I_{Cdl}\,I_f\sin\left(\varphi_f\right)} = \sqrt{X_1 + I_{Cdl}^{\,2}} \tag{10b}
$$

$$
\text{with } X_1 = \frac{\left(\dfrac{n^2F^2A\Gamma_{max}}{RT}\right)^2}{\left(\dfrac{1}{ko\,\chi}\right)^2 + \left(\dfrac{\xi}{w\,\chi}\right)^2}\left(1 + 2Cdl\,\frac{RT}{n^2F^2A\Gamma_{max}}\frac{\xi}{\chi}\right)E_{AC}^{\,2}
$$

In previous work[24], $k_0$ was estimated by plotting the ratio of the magnitude of the peak current ($I_{tot}$) to the magnitude of the background current ($I_{OFF}$) of ACV experiments as a function of the logarithm of the frequency (f) followed by the fitting the sigmoid curve obtained and describing a cut-off phenomenon. Creager and Wooster's performed the same with an approach that does not consider interactions between grafted molecules[14].

The following part aims at expressing $\varphi_{tot}$ with $\chi$ and $\xi$ parameters.

## 4. Theoretical study of the phase angle and analysis

In order to express $\varphi_{tot}$ vs. frequency, its dependence with $\theta_O$ and thus with $\chi$ and $\xi$ must be clearly defined.

Via the common trigonometric formulas, the resultant current expressed with equation 9 can be expanded to:

$$I_{tot}\sin(wt+\varphi_{tot}) = I_{Cdl}\sin(wt+\varphi_{Cdl}) + I_f\sin(wt+\varphi_f)$$

$$I_{tot}\sin(wt+\varphi_{tot}) = I_{Cdl}\left(\sin(wt)\cos(\varphi_{Cdl}) + \cos(wt)\sin(\varphi_{Cdl})\right) + I_f\left(\sin(wt)\cos(\varphi_f) + \cos(wt)\sin(\varphi_f)\right)$$

$$I_{tot}\sin(wt+\varphi_{tot}) = \cos(wt)\left(I_{Cdl}\sin(\varphi_{Cdl}) + I_f\sin(\varphi_f)\right) + \sin(wt)\left(I_{Cdl}\cos(\varphi_{Cdl}) + I_f\cos(\varphi_f)\right) \quad (11)$$

$$I_{tot}\sin(wt+\varphi_{tot}) = A\cos(wt) + B\sin(wt) \quad \text{with} \quad \begin{cases} A = \left(I_{Cdl}\sin(\varphi_{Cdl}) + I_f\sin(\varphi_f)\right) = I_{Cdl} + I_f\sin(\varphi_f) \\ B = \left(I_{Cdl}\cos(\varphi_{Cdl}) + I_f\cos(\varphi_f)\right) = I_f\cos(\varphi_f) \end{cases}$$

From the following equations,

$$\begin{cases} \dfrac{A}{I_{tot}} = \sin(\varphi_{tot}) \\ \dfrac{B}{I_{tot}} = \cos(\varphi_{tot}) \end{cases} \text{ and } \begin{cases} \tan(\varphi_{tot}) = \dfrac{A}{B} \\ I_{tot} = \sqrt{A^2+B^2} \end{cases} \text{ with } \begin{cases} \tan(\varphi_{tot}) = \dfrac{\sin(\varphi_{tot})}{\cos(\varphi_{tot})} \\ \sin^2(\varphi_{tot}) + \cos^2(\varphi_{tot}) = 1 \end{cases} \quad (12)$$

and with equation 11, $\varphi_{tot}$ can be extracted according to:

$$\tan(\varphi_{tot}) = \frac{A}{B} = \frac{I_{Cdl} + I_f\sin(\varphi_f)}{I_f\cos(\varphi_f)} = \frac{I_{Cdl} + I_f\sin\left(\arctan\left(\frac{k_0\,\xi}{w}\right)\right)}{I_f\cos\left(\arctan\left(\frac{k_0\,\xi}{w}\right)\right)} \quad \text{and with} \quad \begin{cases} \sin(\arctan(x)) = \dfrac{x}{\sqrt{1+x^2}} \\ \cos(\arctan(x)) = \dfrac{1}{\sqrt{1+x^2}} \end{cases}$$

$$\tan(\varphi_{tot}) = \frac{I_{Cdl}\sqrt{1+\left(\frac{k_0\,\xi}{w}\right)^2} + I_f\frac{k_0\,\xi}{w}}{I_f}$$

$$\tan(\varphi_{tot}) = \frac{w\,Cdl\,E_{AC}\sqrt{1+\left(\frac{k_0\,\xi}{w}\right)^2}}{P\,E_{AC}\sqrt{\left(\frac{1}{ko\,\chi}\right)^2+\left(\frac{\xi}{w\,\chi}\right)^2}} + \frac{k_0\,\xi}{w} \quad \text{with} \quad P = \frac{n^2F^2A\Gamma_{max}}{RT} \quad (13)$$

And, finally, after some tricky rearrangements to:

$$\tan(\varphi_{tot}) = \frac{k_0\,\xi}{w} + \frac{Cdl}{P}\frac{\xi^2}{\chi}\frac{k_0}{w} + \frac{Cdl}{P}\frac{1}{\chi}\frac{w}{k_0} \quad (14)$$

Equation 14 shows that $\varphi_{tot}$ depends on the ratio $k_0/w$, Cdl, and $\chi$ and $\xi$ parameters in which interaction parameters (G, S, $a_{ij}$) are included.

From the possible values of the parameters of this equation, the values of $\varphi_{tot}$ are located between π/2 (capacitive behaviour when w tends to 0 or infinity) and 0. In this case, the trends of $\varphi_{tot}$ and $\tan(\varphi_{tot})$ are the same, so future interpretations of the results will be conducted on either of these parameters.

$\varphi_{tot}$ vs. {$\theta_O$ and frequency} calculated from equation 14 for two specific combinations {$k_0$ ; $a_{OO}$ ; Cdl ; $\theta_T$} = {100 $s^{-1}$ ; 0 or 1 ; 5 µF ; 1} is strongly impacted by the presence of interactions between redox species as seen in figure 2A. This results from the huge modification of the expressions and trends of $\chi$ and $\xi$ which lose their axis of symmetry in $\theta_O = \frac{\theta}{2}$. The same analogy can be made with the $I_{tot}$ variation vs. {$\theta_O$ and frequency}

Figure 2B and 2C provide evidence of the complexity of the phenomena involved: a loss of the proportionality of the variation of $\varphi_{tot}$ at different $\theta_O$ or frequencies, boundary effects and a shift of local minima (ON and ON* - magenta and blue crosses respectively). For example, in the absence of interaction, whatever $\theta_O$, local ON* minima are located close to the same frequency (not true for $\theta_O \to 0$ or 1 - pink dot line), and inversely whatever the frequency, local ON minima are always located at the same $\theta_O = \frac{\theta}{2}$, which is not the case when interactions exist. However, there is always a single remarkable point, which is both an ON state and an ON* state, corresponding to the smallest phase angle called $\varphi_{Min}$ for a single pair $\{\theta_{O,\varphi_{Min}}; f_{\varphi_{Min}}\}$, all three depending in value on the parameters involved in equation 14.

At given frequencies, if we compare the trends of $I_{tot}/I_{OFF}$ and $\varphi_{tot}$ vs. $\theta_O$ (figure 2B, SI-1) in the presence of interactions, some similarities are observed with the presence of inflexion point, the ON states at $\{\theta_{O,I_{ON}}; I_{ON}\}$ and $\{\theta_{O,\varphi_{ON}}; \varphi_{ON}\}$ (a maximum $I_{ON}$ for $I_{tot}$ and a minimum $\varphi_{ON}$ for $\varphi_{tot}$ - see equation 4b), but their respective values ($\theta_{O,I_{ON}}$ and $\theta_{O,\varphi_{ON}}$) are clearly not located at the same values (figure 3, SI-2). Indeed, for any values of the interaction coefficients ($a_{OO}$) and of Cdl, $\theta_{O,I_{ON}}$ is always equal, for low frequencies, to a specific value of $\theta/2$, which is not the case for $\theta_{O,\varphi_{ON}}$, which does not present any invariant point. Another point, already observed for $\theta_{O,I_{ON}}$, is the sigmoid dependence of $\theta_{O,\varphi_{ON}}$ *vs.* log(frequency) which produces the well-known cut-off phenomenon according to parameters involved in equation 14, with two plateaux at low and high frequencies. In all cases, $\varphi_{ON}$ and $\theta_{O,\varphi_{ON}}$ are greatly influenced by the values of interaction parameters and Cdl.

At a given $\theta_O$ (i.e., potential), the $\varphi_{tot}$ vs. frequency plots (figure 2C) exhibit inflexion points, the ON* states at $\{f_{\varphi_{ON}^*}; \varphi_{ON}^*\}$. For any values of the interaction coefficients ($a_{OO}$) and of Cdl, $\varphi_{ON}^*$ and $f_{\varphi_{ON}^*}$ are also greatly influenced by the values of interaction parameters and Cdl, but no plateau or constant values of $f_{\varphi_{ON}^*}$, apart from an infinite limit when $\theta_O$ tends to 0 or 1 (figure 4).

Based on these finding, four strategies can be considered to reach $k_0$:

1. Recording $\varphi_{tot}$ at different frequencies for a given $\theta_O$ (i.e., potential), with Multi-frequency AV experiments (same setup as EIS experiments). The curve obtained can be modelled using equation 14. To achieve good accuracy via a curve fitting process of $k_0$, the variation of $\varphi_{tot}$ must be maximized, which means that the experiment must be ideally performed at a special $\theta_O$ that produces the minimum $\varphi_{ON}^*$ i.e. $\varphi_{Min}$.
2. Same strategy as before but carried out at several $\theta_O$. In this case, if the expression of $\varphi_{ON}^*$ can be determined (*vide infra*), the curve fitting process must be performed on this parameter as a function of $f_{\varphi_{ON}^*}$.

3. Recording $\varphi_{tot}$ at several $\theta_O$ at a given frequency, with an ACV experiment (or several AV experiments). The curve obtained can be modelled using equation 14. To achieve good accuracy of $k_0$ via a curve fitting process, the variation of $\varphi_{tot}$ must be maximized, which means that the experiment must be performed at a peculiar frequency that produces the minimum value of $\varphi_{ON}$ i.e. $\varphi_{Min}$.
4. Same approach as before but carried out at several frequencies. In this case, if the expression of $\varphi_{ON}$ can be determined (*vide infra*), the curve fitting process can be carried out on this parameter as a function of $\theta_{O,\varphi_{ON}}$.

## 5. Fitting procedures

### 5.1. At a given potential, as a function of frequency

If the phase angle of the current is recorded at a given potential (i.e. at a given $\theta_O$), $\chi$ and $\xi$ are constant. The phase angle only depends on the ratio $k_0/w$ and Cdl and equation 14 becomes:

$$\tan(\varphi_{tot\{E,\theta_O\}}) = \frac{k_0\,\xi_{\{E,\theta_O\}}}{w} + \frac{Cdl}{P}\frac{\xi^2_{\{E,\theta_O\}}}{\chi_{\{E,\theta_O\}}}\frac{k_0}{w} + \frac{Cdl}{P\chi_{\{E,\theta_O\}}}\frac{w}{k_0} \qquad (15)$$

As $\theta_O$ can be evaluated using GLI function, taking advantage of the $\tan(\varphi_{tot\{E,\theta_O\}})$ vs w plot via a curve fitting procedure makes it possible to estimate $k_0$ and Cdl in one shot (strategy 1). This strategy is optimal if the variation of $\tan(\varphi_{tot\{E,\theta_O\}})$ is maximal during the experiment: this requires estimating the value of $\theta_O$ that produce $\varphi_{Min}$.

Firstly, we need to reach the frequency at $\varphi^*_{ON\{E,\theta_O\}}$, after finding the zeros (Appendix B) of the derivative of equation 15 with respect to w:

$$w^*_{\varphi_{ON\{E,\theta_O\}}} = k_0\,\xi_{\{E,\theta_O\}}\sqrt{1+\frac{P\chi_{\{E,\theta_O\}}}{Cdl\,\xi_{\{E,\theta_O\}}}} \qquad (16)$$

At $w^*_{\varphi_{ON\{E,\theta_O\}}}$, equation 14 becomes:

$$\tan(\varphi^*_{ON\{E,\theta_O\}}) = 2\sqrt{\frac{Cdl\,\xi_{\{E,\theta_O\}}}{P\chi_{\{E,\theta_O\}}}\left(1+\frac{Cdl\,\xi_{\{E,\theta_O\}}}{P\chi_{\{E,\theta_O\}}}\right)} \qquad (17a)$$

$$\tan(\varphi^*_{ON\{E,\theta_O\}}) = 2\,\frac{Cdl}{P\chi_{\{E,\theta_O\}}}\frac{w^*_{\varphi_{ON\{E,\theta_O\}}}}{k_0} \qquad (17b)$$

Secondly, $\varphi_{Min}$ is reach by finding the zeros of the derivative of equation 17a with respect to $\theta_O$ (Appendix B). It is noteworthy that, whatever the interaction coefficients and Cdl, $\varphi_{Min}$ is always reached when $\theta_{O,\varphi_{Min}} = \theta/2$ (i.e. at $E = E_p = E^{0'} + \frac{RT}{nF}\theta S$) and therefore easy to implement experimentally.

If we perform this experiment at several given potentials, it is possible to determine $k_0$ from the ON* states (Strategy 2). Keeping in mind that $\theta_O$ is determined via the GLI function, fitting the $\tan(\varphi^*_{ON\{E,\theta_O\}})$ vs $\theta_O$ plot via equation 17a and the $\tan(\varphi^*_{ON\{E,\theta_O\}})$ vs $w_{\varphi^*_{ON\{E,\theta_O\}}}$ plot via equation 17b lead to estimate Cdl and $k_0$ in one shot respectively. A more attractive option is to proceed directly to the curve fitting procedure on $\tan(\varphi^*_{ON\{E,\theta_O\}})$ vs $\{ w_{\varphi^*_{ON\{E,\theta_O\}}}$ and $\theta_O \}$ for determining $k_0$ and Cdl in one shot via equation 15.

### 5.2. At a given frequency, as a function of potential

At a given frequency (w) during an AV, the phase angle variation only depends on the on $\chi$ and $\xi$, i.e. $\theta_O$ and equation 14 becomes:

$$\tan(\varphi_{tot\{w\}}) = \frac{k_0}{w}\xi + \frac{Cdl}{P}\frac{\xi^2}{\chi}\frac{k_0}{w} + \frac{Cdl}{P\chi}\frac{w}{k_0} \qquad (18)$$

As $\theta_O$ can be evaluated using GLI function, fitting the $\tan(\varphi_{tot\{w\}})$ vs $\theta_O$ plot via equation 18 makes it possible to estimate $k_0$ and Cdl in one shot (strategy 3). As with strategies 1, this strategy is optimal if the variation of $\tan(\varphi_{tot\{E,\theta_O\}})$ is maximal during the experiment: this requires estimating a frequency that produces $\varphi_{Min}$.

Firstly, finding the zeros of the derivative of equation 18 with respect to $\theta_O$ allows to reach $\theta_O$ at $\varphi_{ON\{w\}}$ (i.e. a specific couple ( $\chi$ ; $\xi$ )). Mathematically complex with the presence of non-linearities, solutions can only be found at boundary conditions ( $w \to 0$ or $w \to \infty$ ), i.e., plateaux observed in figure 3:

- $$\frac{w}{k_0} \to \infty \;\Rightarrow\; \lim_{w/k_0 \to \infty}\left(\tan(\varphi_{tot})\right) = \frac{Cdl}{P}\frac{1}{\chi}\frac{w}{k_0} \;\Rightarrow\; \theta_{O,\varphi_{ON},w/k_0 \to \infty} = \frac{S\theta + \sqrt{S^2\theta^2+1}-1}{2S} \qquad (19)$$

  whose step-by-step development is detailed in Appendix C.

- $$\frac{w}{k_0} \to 0 \;\Rightarrow\; \lim_{w/k_0 \to 0}\left(\tan(\varphi_{tot})\right) = \frac{k_0}{w}\xi + \frac{Cdl}{P}\frac{\xi^2}{\chi}\frac{k_0}{w} \;\Rightarrow\; \theta_{O,\varphi_{ON},w/k_0 \to 0} = f\left(\theta;G;S;Cdl\right)$$

  whose value very influenced by interactions and Cdl can be determined in some conditions ( $Cdl \to 0$ or $\infty$ ) by Ferrari's and Cardan's method and whose step-by-step development produces an oversize equation[31].

Consequently, this approach (strategy 3), while usable, is not optimal because it does not allow access to the best frequency to perform the experiment and therefore to estimate $k_0$ with the highest accuracy. An approximate frequency can nevertheless be estimated by first carrying out strategy 1 at $\theta_{O,\varphi_{Min}} = \theta/2$, which makes it possible to determine experimentally $f_{\varphi_{Min}}$ at $\varphi_{Min}$.

If we perform this experiment at several given frequencies, it is possible to determine $k_0$ from the ON states (strategy 4). Keeping in mind that $\theta_O$ is determined via the GLI function, it is possible to proceed the fitting of $\tan(\varphi_{ON\{w\}})$ with respect to $\theta_{O,\varphi_{ON\{w\}}}$ and w using equation 18 for determining $k_0$ and Cdl in one shot.

Figure 5 highlights the principle of these strategies and shows the results of the curve fitting procedure and the estimation of $k_0$ and Cdl using simulated alternative voltammograms with $a_{OO}$=1, $k_0$=100 $s^{-1}$ and Cdl=5 µF as input parameters.

These four fitting procedures makes it possible to determine the values of $k_0$ and Cdl with good accuracies and precisions in the case of interacting electroactive species.

These strategies were also tested with a lower number of points and with an added Gaussian noise (SI-3), and showed that strategies 1 and 3 remain the most robust under these conditions, which is explained by the fact that the fit uses only one variable as input (frequency for strategy 1 and $\theta_O$ for strategy 3) and not both simultaneously for strategy 2 and 4.

## 6. Fitting procedures on experimental data

### 6.1. Measurement feasibility

Equations describing the monitored parameters of an AV or ACV experiment ($I_{tot}$ and $\varphi_{tot}$) are based on Randles model assuming a sinusoidal response to a sinusoidal solicitation. As for the amplitude of the current ($I_{tot}$), where a very low potential amplitude ($E_{AC}$) and therefore a very low scan rate (v) are required, some parameters must also be finely controlled to obtain a reliable measurement of the phase angle $\varphi_{tot}$ in agreement with the assumptions of the Randle's model and to be able to use the strategies proposed previously.

The number of points per cycle is the first critical point. As the phase angle is directly related to a time difference between the applied potential and the resulting current, the minimum resolution of the phase angle measurement therefore depends on the time base used (Δt) to increment the potential, which is a function of the number of points per cycle (N) and the frequency of the AC component. Consequently, and whatever the numerical determination method chosen (search for the maximum, offset of the power component, correlation of the signals e(t) and i(t)…), the phase angle resolution is the measurement of two adjacent points by:

$$R_\varphi = 2\pi f \Delta t = \frac{2\pi}{N} \qquad \text{with } \Delta t = \frac{1}{N \cdot f} \qquad 20)$$

According to equation 20, $\varphi_{tot}$ measurement resolution depends mainly on the number of points per cycle. The accurate measurement of small changes in the phase angle can therefore only be achieved by increasing the number of points, which leads to digitization problems even for newer potentiostats. The phase angle resolution dependence with N is clearly observed in figure 6A, where for example with N=36 a resolution $R_\varphi$ =0.175 is insufficient to finely measure $\varphi_{tot}$ variations.

Determination of $\theta_{O,\varphi_{ON}}$ and $w_{\varphi_{ON}}$ are also strongly impacted by the number of points, especially when the variation of $\varphi_{tot}$ is small around these points. For example, in figure 6A, for N=36, $\theta_{O,\varphi_{ON}}$ is in a wide interval between 0.45 and 0.69.

The potential amplitude ($E_{AC}$) is the second critical point. The lower this factor is, the closer the induced current will be close to a perfect sinusoid and therefore to the theoretical results based on a linear response of the system. $\varphi_{tot}$ measurement accuracy dependence with $E_{AC}$ is clearly observed in figure 6B, a convergence taking place by progressively decreasing the value of $E_{AC}$.
A low potential amplitude and therefore the use of a low scan rate (v) is required to avoid excessive distortion of the AC voltammograms (see 3.3). $E_{AC}$ must nevertheless be large enough to measure a resulting current, which requires some compromises.

In conclusion, access to $\varphi_{tot}$ remains a challenge in an AV or ACV experiment, requiring the system to be placed in restricted conditions (low potential amplitude, near zero scan rate and large number of points). With these technical considerations, the most appropriate measurement strategies will be chosen according to the characteristics of the potentiostat used to obtain experimentally accurate measurements with an acceptable number of points.

### 6.2. Theory vs. experience

To validate the above approaches, the frequency dependence of the phase angle in Alternative Voltammetry was studied through TEMPO-based SAMs (C15-TEMPO) on Au substrate, a well-known redox-responsive material. Indeed, previous works[27,32] shown that the analysis of CVs at different surface coverages under reversible conditions allows with the extraction of characteristic parameters such as the full width at half maximum (FWHM), peak potential (Ep) and peak intensity (ip) to quantify (with equation 1) the interactions between the adsorbed electroactive species. Associated to the knowledge of the chemical system involved (electrochemical system, isotherms of immobilization in the neutral state ...), the interaction parameters G, S and $a_{OO}$ of TEMPO-based SAMs were estimated at 1, -1 and 1 respectively. Figure 7A shows an experimental cyclic voltammogram of a TEMPO SAM presenting a surface coverage of electroactive species of 2.8 $10^{-10}$ mol.cm$^{-2}$ (i.e., $\theta = \frac{\Gamma}{\Gamma_{max}} = \frac{2.8 \cdot 10^{-10}}{5 \cdot 10^{-10}} = 0.62$ with a mean value of $\Gamma_{max}$ according to references [22,24,26,29]) and a peak potential $E_p$ closed to 0.820 V vs Ag reference electrode, on which alternative experiment will be performed hereafter.

In order to comply with the feasibility criteria and avoid measurement bias caused by different techniques, the experiments were carried out under the same conditions constrained by the potentiostat used (BIOLOGIC SP300):

- Alternative Voltammetry at a fixed potential ($E_{DC}$) and fixed frequency
- Temporal acquisition resolution $\Delta t_{acq}$= 0.5 ms
- $R_{\varphi} = 2\pi f \Delta t_{acq}$, that induces a poor resolution at high frequency
- 10 measurements cycles after a stabilization at $E_{DC}$ during 15s
- Amplitude of the sinusoidal part, $E_{AC}$ = 1 mV

Here are the ranges used in $\theta$ and in frequency:

- $\theta$ : 20 points around $E_p$ with a step of 5 mV, which are transformed into $\theta$ using the GLI function (equation 2)
- Frequency: points from 1 Hz to 500 Hz with 3 points per decade regularly spaced logarithmically

Note that strategies 2 and 4 cannot be tested on TEMPO SAMs because these approaches require long experimental times and then very stable redox-responsive materials. For all the experiments of strategies 1 and 3, the phase angles were determined by correlation between e(t) and i(t), this method being the most accurate in the presence of noisy signals.

Figure 7B displays, as example, an experimental alternative voltammogram of the same TEMPO-SAM performed at the peak potential ($\theta_O = \theta/2 = 0.31$) and at a frequency of 10 Hz. Once steady state is obtained after two cycles, this alternative voltammogram gives a phase angle around 1.35 rad ($\varphi = 2\pi f \Delta t$). This same procedure repeated at several frequencies makes it possible to obtain figure 7C (strategy 1). Figure 7D (strategy 3) is obtained at a fixed frequency of 50 Hz to be sure of obtaining acceptable measurement resolution ($R_\varphi = 0.063$) and phase angle variation (~0.70 rad), while this frequency is not the one allowing $\varphi_{Min}$ to be obtained at $f_{\varphi_{Min}}$ estimated close to 200 Hz (but with an unacceptable $R_\varphi = 0.251$).

Figure 7C and 7D show a good agreement of the experimental plots with the theory proposed and allow to estimate the parameters $k_0$ and $C_{dl}$ via a fitting procedure with a good accuracy and precision (Table 2).
The two strategies give quite similar results, strategy 1 being the most robust, especially on the accuracy of Cdl. Table 2 also shows the estimations made without considering the interactions. In this case, the results are not representative given the accuracy of the estimated values ($S_{k0}$ and $S_{Cdl}$) and prove the usefulness of the proposed model which takes the interactions into account.
In addition, all the results obtained with these two fitting procedures are compared with those obtained with the procedures described in the previous article and based on the ratio of $I_{tot}/I_{OFF}$.
The results estimated for $k_0$ are quite similar (value and accuracy), and those found for Cdl are less precise compared to previous method despite fairly close estimated values, the slight differences observed can be explained by the environment, the difference between the batches and the stability of the SAMs.
This proves the validity of this phase angle model, even if it remains more difficult to implement with current technologies and involves the use of a very powerful instrument.

**8. Conclusion**

Accurately estimating the standard electrochemical rate constant ($k_0$) for heterogeneous electron transfer reactions in the case of strong intermolecular interactions occur between the redox forms is therefore possible by following the phase angle during of AV experiments.
The validity of our methodological approach has been demonstrated experimentally on TEMPO-based SAMs and compared with previous results, but it must be emphasized that it remains difficult to implement with current technologies and implies the use of a potentiostat with a reliable frequency response analyzer.
At last, this methodology also confirms our previous work based on the $I_{ON}/I_{OFF}$ ratio.

**Acknowledgments**

The authors thank Flavy ALEVEQUE for her critical reading of the manuscript, Dr. Christelle GAUTIER for the synthesis of TEMPO-based molecules and the plateau CARMA of the SFR MATRIX (University of ANGERS) for the spectroelectrochemical characterisations.

**Appendices**

**Appendix A**

**A1**

Via the common trigonometric formulas, the resultant current expressed with equation 9 can be expanded to:

$$\left.\begin{aligned} &_{tot}\sin\left(wt+\varphi_{tot}\right)=I_{Cdl}\sin\left(wt+\varphi_{Cdl}\right)+I_f\sin\left(wt+\varphi_f\right)\\ &I_{tot}\sin\left(wt+\varphi_{tot}\right)=I_{Cdl}\left(\sin\left(wt\right)\cos(\varphi_{Cdl})+\cos\left(wt\right)\sin(\varphi_{Cdl})\right)+I_f\left(\sin\left(wt\right)\cos\left(\varphi_f\right)+\cos\left(wt\right)\sin\left(\varphi_f\right)\right)\\ &I\,I_{tot}\sin\left(wt+\varphi_{tot}\right)=\cos\left(wt\right)\left(I_{Cdl}\sin(\varphi_{Cdl})+I_f\sin\left(\varphi_f\right)\right)+\sin\left(wt\right)\left(I_{Cdl}\cos(\varphi_{Cdl})+I_f\cos\left(\varphi_f\right)\right)\\ &I_{tot}\sin\left(wt+\varphi_{tot}\right)=A\cos\left(wt\right)+B\sin\left(wt\right)\quad\text{with}\quad\begin{cases}A=\left(I_{Cdl}\sin(\varphi_{Cdl})+I_f\sin\left(\varphi_f\right)\right)=I_{Cdl}+I_f\sin\left(\varphi_f\right)\\ B=\left(I_{Cdl}\cos(\varphi_{Cdl})+I_f\cos\left(\varphi_f\right)\right)=I_f\cos\left(\varphi_f\right)\end{cases}\end{aligned}\right\}\quad\text{(A1)}$$

Via trigonometric formulas:

$$\begin{cases}\dfrac{A}{I_{tot}}=\sin(\varphi_{tot})\\ \dfrac{B}{I_{tot}}=\cos(\varphi_{tot})\end{cases}\quad\text{and}\quad\begin{cases}\tan(\varphi_{tot})=\dfrac{A}{B}\\ I_{tot}=\sqrt{A^2+B^2}\end{cases}\quad\text{with}\quad\begin{cases}\tan(\varphi_{tot})=\dfrac{\sin(\varphi_{tot})}{\cos(\varphi_{tot})}\\ \sin^2(\varphi_{tot})+\cos^2(\varphi_{tot})=1\end{cases}\quad\text{(A2)}$$

$I_{tot}$ can be determined combining A1 and A2:

$$\begin{aligned}&I_{tot}=\sqrt{A^2+B^2}=\sqrt{\left(I_{Cdl}+I_f\sin\left(\varphi_f\right)\right)^2+\left(I_f\cos\left(\varphi_f\right)\right)^2}\\ &I_{tot}=\sqrt{{I_f}^2+{I_{Cdl}}^2+2I_{Cdl}I_f\sin\left(\varphi_f\right)}=\sqrt{X_1+{I_{Cdl}}^2}\qquad\text{with}\qquad X_1={I_f}^2+2I_{Cdl}I_f\sin\left(\varphi_f\right)\end{aligned}\quad\text{(A3)}$$

**A2**

$$\begin{cases}I_{Cdl}=w\,Cdl\,E_{AC}\\ \varphi_{Cdl}=\dfrac{\pi}{2}\end{cases}\quad\text{and}\quad\begin{cases}\varphi_f=\arctan\left(\dfrac{k_0\,\xi}{w}\right)\\ If=\dfrac{P\,E_{AC}}{\sqrt{\left(\dfrac{1}{ko\,\chi}\right)^2+\left(\dfrac{\xi}{w\,\chi}\right)^2}}\end{cases}\quad\text{with }P=\frac{n^2F^2A\Gamma_{max}\theta}{RT}\quad\text{(A4)}$$

from equation A4

$$\sin\left(\varphi_f\right)=\sin\left(\arctan\left(\frac{k_0\,\xi}{w}\right)\right)=\frac{k_0\,\xi}{\sqrt{\left(k_0\,\xi\right)^2+\left(w\right)^2}}\quad\text{(A5)}$$

And by combining A3 and A5

$$X_1={I_f}^2\left(1+2\frac{I_{Cdl}}{I_f}\sin\left(\varphi_f\right)\right)$$

$$X_1 = \left( \frac{P E_{AC}}{\sqrt{\left(\frac{1}{k_0\,\chi}\right)^2 + \left(\frac{\xi}{w\,\chi}\right)^2}} \right)^2 \left( 1 + \frac{2\,w\,Cdl\,E_{AC}\,\frac{k_0\,\xi}{\sqrt{\left(\left(k_0\,\xi\right)^2 + \left(w\right)^2\right)}}}{\frac{P E_{AC}}{\sqrt{\left(\frac{1}{k_0\,\chi}\right)^2 + \left(\frac{\xi}{w\,\chi}\right)^2}}} \right)$$

$$X_1 = \frac{P^2}{\left(\frac{1}{ko\,\chi}\right)^2 + \left(\frac{\xi}{w\,\chi}\right)^2} \left( 1 + \frac{2\,Cdl}{P}\,\frac{\xi}{\chi} \right) {E_{AC}}^2 \qquad \text{(A6)}$$

**Appendix B**

**B1**

$$\tan(\varphi_{tot\{E,\theta_O\}}) = \frac{k_0\,\xi_{\{E,\theta_O\}}}{w} + \frac{Cdl}{P}\,\frac{\xi^2_{\{E,\theta_O\}}}{\chi_{\{E,\theta_O\}}}\,\frac{k_0}{w} + \frac{Cdl}{P\,\chi_{\{E,\theta_O\}}}\,\frac{w}{k_0} \qquad \text{(B1)}$$

$$\frac{d\left(\tan(\varphi_{tot\{E,\theta_O\}})\right)}{dw} = -\frac{k_0\,\xi_{\{E,\theta_O\}}}{w^2} - \frac{Cdl}{P}\,\frac{\xi^2_{\{E,\theta_O\}}}{\chi_{\{E,\theta_O\}}}\,\frac{k_0}{w^2} + \frac{Cdl}{P\,\chi_{\{E,\theta_O\}}\,k_0} \qquad \text{(B2)}$$

$$\frac{d\left(\tan(\varphi_{tot\{E,\theta_O\}})\right)}{dw} = 0 \quad \text{at} \quad \varphi^*_{ON\{E,\theta_O\}} \qquad \text{(B3)}$$

$${w_{\varphi^*_{ON\{E,\theta_O\}}}}^2 = \frac{P\,\chi_{\{E,\theta_O\}}\,\xi_{\{E,\theta_O\}}}{Cdl}\,{k_0}^2 + \xi^2_{\{E,\theta_O\}}\,{k_0}^2 \qquad \text{(B4)}$$

$$w_{\varphi^*_{ON\{E,\theta_O\}}} = k_0\,\xi_{\{E,\theta_O\}}\sqrt{1 + \frac{P\,\chi_{\{E,\theta_O\}}}{Cdl\,\xi_{\{E,\theta_O\}}}} \qquad \text{(B5)}$$

By combining (B1) and (B5),

$$\tan(\varphi^*_{ON\{E,\theta_O\}}) = \frac{k_0\,\xi_{\{E,\theta_O\}}}{w_{\varphi^*_{ON\{E,\theta_O\}}}} + \frac{Cdl}{P}\,\frac{\xi^2_{\{E,\theta_O\}}}{\chi_{\{E,\theta_O\}}}\,\frac{k_0}{w_{\varphi^*_{ON\{E,\theta_O\}}}} + \frac{Cdl}{P\,\chi_{\{E,\theta_O\}}}\,\frac{w_{\varphi^*_{ON\{E,\theta_O\}}}}{k_0} \qquad \text{(B6)}$$

$$\tan(\varphi^*_{ON\{E,\theta_O\}}) = \left[ \begin{array}{l} \dfrac{1}{\sqrt{1 + \dfrac{P\,\chi_{\{E,\theta_O\}}}{Cdl\,\xi_{\{E,\theta_O\}}}}} + \\ \dfrac{Cdl}{P}\,\dfrac{\xi_{\{E,\theta_O\}}}{\chi_{\{E,\theta_O\}}}\,\dfrac{1}{\sqrt{1 + \dfrac{P\,\chi_{\{E,\theta_O\}}}{Cdl\,\xi_{\{E,\theta_O\}}}}} + \\ \dfrac{Cdl\,\xi_{\{E,\theta_O\}}}{P\,\chi_{\{E,\theta_O\}}}\sqrt{1 + \dfrac{P\,\chi_{\{E,\theta_O\}}}{Cdl\,\xi_{\{E,\theta_O\}}}} \end{array} \right] \qquad \text{(B7)}$$

$$\tan(\varphi^{*}_{ON\{E,\theta_O\}}) = \left[ \begin{array}{c} \dfrac{Cdl\ \xi_{\{E,\theta_O\}}}{\sqrt{Cdl\ \xi_{\{E,\theta_O\}}\left(Cdl\ \xi_{\{E,\theta_O\}} + P\chi_{\{E,\theta_O\}}\right)}} + \\ \dfrac{Cdl^2\ \xi^2_{\{E,\theta_O\}}}{P\chi_{\{E,\theta_O\}}\sqrt{Cdl\ \xi_{\{E,\theta_O\}}\left(Cdl\ \xi_{\{E,\theta_O\}} + P\chi_{\{E,\theta_O\}}\right)}} + \\ \dfrac{\sqrt{Cdl\ \xi_{\{E,\theta_O\}}\left(Cdl\ \xi_{\{E,\theta_O\}} + P\chi_{\{E,\theta_O\}}\right)}}{P\ \chi_{\{E,\theta_O\}}} \end{array} \right] \tag{B8}$$

$$\tan(\varphi^{*}_{ON\{E,\theta_O\}}) = 2\sqrt{\frac{Cdl\ \xi_{\{E,\theta_O\}}}{P\chi_{\{E,\theta_O\}}}\left(1+\frac{Cdl\ \xi_{\{E,\theta_O\}}}{P\chi_{\{E,\theta_O\}}}\right)} \tag{B9}$$

and by combining (B9) and (B5), (B9) can also be written,

$$\tan(\varphi^{*}_{ON\{E,\theta_O\}}) = 2\frac{Cdl\ \xi_{\{E,\theta_O\}}}{P\chi_{\{E,\theta_O\}}}\sqrt{1+\frac{P\chi_{\{E,\theta_O\}}}{Cdl\ \xi_{\{E,\theta_O\}}}} = 2\frac{Cdl}{P\chi_{\{E,\theta_O\}}}\frac{w_{\varphi^{*}_{ON\{E,\theta_O\}}}}{k_0} \tag{B10}$$

**B2**

$$\begin{cases} \chi = \sqrt{\theta_O\theta_R}\,e^{-\theta_O(a_{OO}+a_{OR})-\theta_R(a_{RR}+a_{OR})} = \sqrt{\theta_O(\theta-\theta_O)}\,e^{\theta_O S-\theta(a_{RR}+a_{OR})} \\ \xi = \chi\dfrac{\theta-2G\theta_O\theta_R}{\theta_O\theta_R} = \chi\dfrac{\theta-2G\theta_O(\theta-\theta_O)}{\theta_O(\theta-\theta_O)} \\ \dfrac{\xi}{\chi} = \dfrac{\theta-2G\theta_O(\theta-\theta_O)}{\theta_O(\theta-\theta_O)} \end{cases} \tag{B11}$$

$\varphi^{*}_{ON\{E,\theta_O\}} \in \left[0\ ;\ \frac{\pi}{2}\right]$, which means that the trend of $\tan(\varphi^{*}_{ON\{E,\theta_O\}})$ is like the trend of $\tan^2(\varphi^{*}_{ON\{E,\theta_O\}})$

$$\tan^2(\varphi^{*}_{ON\{E,\theta_O\}}) = 4\frac{Cdl\ \xi_{\{E,\theta_O\}}}{P\chi_{\{E,\theta_O\}}}\left(1+\frac{Cdl\ \xi_{\{E,\theta_O\}}}{P\chi_{\{E,\theta_O\}}}\right) = 4\frac{Cdl}{P}\frac{\theta-2G\theta_O(\theta-\theta_O)}{\theta_O(\theta-\theta_O)}\left(1+\frac{Cdl}{P}\frac{\theta-2G\theta_O(\theta-\theta_O)}{\theta_O(\theta-\theta_O)}\right) \tag{B12}$$

$$\frac{d\tan^2(\varphi^{*}_{ON\{E,\theta_O\}})}{d\theta_O} = \frac{32Cdl\ \theta}{P^2\left(\theta_O(\theta-\theta_O)\right)^3}\left(\theta_O-\frac{\theta}{2}\right)\left(\left(G\ Cdl-\frac{P}{4}\right)\theta_O{}^2-\theta\left(G\ Cdl-\frac{P}{4}\right)\theta_O+\frac{\theta\ Cdl}{2}\right) \tag{B13}$$

$$\frac{d\tan^2(\varphi^{*}_{ON\{E,\theta_O\}})}{d\theta_O} = 0 \quad \text{at} \quad \varphi_{Min} \tag{B14}$$

Zero of the red part is $\theta_O = \frac{\theta}{2}$ (B15)

Zeros of the blue part are $\theta_O = \dfrac{(4CdlG-P)\theta \pm \sqrt{(4CdlG-P)^2\theta^2 - 8\theta Cdl(4CdlG-P)}}{2(4CdlG-P)}$ (B16)

Some conditions are necessary to validate the zeros obtained in (B16).

Case 1: $(4CdlG-P) > 0$

In this case, $G > \frac{P}{4Cdl} > 0$

Solutions between 0 and $\theta$ are obtained if:

$$\begin{cases} 0 < \sqrt{(4CdlG-P)^2\theta^2 - 8\theta Cdl(4CdlG-P)} < (4CdlG-P)\theta \\ P > 0\ ;\ Cdl > 0\ ;\ \theta > 0 \end{cases}$$

The upper condition is true.

The lower condition is not true because:

$$(4CdlG-P)^2\theta^2 - 8\theta Cdl(4CdlG-P) > 0$$
$$(4CdlG-P)\theta - 8Cdl > 0$$
$$Cdl(4G\theta - 8) - P\theta > 0$$

$$Cdl < \frac{P\theta}{4G\theta - 8} < 0 \quad \text{with} \begin{cases} P\theta > 0 \\ 4G\theta - 8 < 0 \text{ with } G \in [-2\ ;\ 2] \text{ and } \theta \in [0\ ;\ 1] \end{cases}$$

Cdl cannot be positive, that is impossible.

<u>Case 2:</u> $(4CdlG-P) < 0$

In this case, $G < \frac{P}{4Cdl}$

Solutions between 0 and $\theta$ are obtained if:

$$\begin{cases} \sqrt{(4CdlG-P)^2\theta^2 - 8\theta Cdl(4CdlG-P)} > 0 > (4CdlG-P)\theta \\ P > 0\ ;\ Cdl > 0\ ;\ \theta > 0 \end{cases}$$

$$(4CdlG-P)^2\theta^2 - 8\theta Cdl(4CdlG-P) > 0$$
$$(4CdlG-P)\theta - 8Cdl < 0$$
$$Cdl(4G\theta - 8) - P\theta < 0$$

$$Cdl < \frac{P\theta}{4G\theta - 8} < 0 \quad \text{with} \begin{cases} P\theta > 0 \\ 4G\theta - 8 < 0 \text{ with } G \in [-2\ ;\ 2] \text{ and } \theta \in [0\ ;\ 1] \end{cases}$$

Cdl cannot be positive, that is impossible.

At last, $\theta_O = \frac{\theta}{2}$ (B15) is the unique solution

**Appendix C**

$$\tan(\varphi_{tot\{w\}}) = \frac{k_0\,\xi}{w} + \frac{Cdl}{P}\frac{\xi^2}{\chi}\frac{k_0}{w} + \frac{Cdl}{P\chi}\frac{w}{k_0} \qquad (C1)$$

$$\frac{w}{k_0} \to \infty \;\Rightarrow\; \lim_{w/k_0 \to \infty}\left(\tan(\varphi_{tot})\right) = \frac{Cdl}{P}\frac{1}{\chi}\frac{w}{k_0} \tag{C2}$$

$$\frac{d\tan(\varphi_{tot})}{d\theta_O} = \frac{Cdl}{P}\frac{w}{k_0}\frac{e^{-\theta_O S-\theta(a_{RR}+a_{OR})}}{\left(\theta_O(\theta-\theta_O)\right)^{3/2}}\left(S\theta_O{}^2+\theta_O(1-S\theta)-\frac{\theta}{2}\right) \tag{C3}$$

$$\frac{d\tan(\varphi_{tot})}{d\theta_O} = 0 \quad \text{at} \quad \varphi_{ON\{w\}} \;\Rightarrow\; \left(S\theta_O{}^2+\theta_O(1-S\theta)-\frac{\theta}{2}\right) = 0 \tag{C4}$$

The only solution between 0 and $\theta$ is

$$\theta_{O,\varphi_{ON},w/k_0\to\infty} = \frac{S\theta+\sqrt{S^2\theta^2+1}-1}{2S} \tag{C5}$$

**References**


[1] R.G. Nuzzo, D.L. Allara, Adsorption of bifunctional organic disulfides on gold surfaces, J. Am. Chem. Soc. 105 (1983) 4481–4483. https://doi.org/10.1021/ja00351a063.

[2] J.C. Love, L.A. Estroff, J.K. Kriebel, R.G. Nuzzo, G.M. Whitesides, Self-Assembled Monolayers of Thiolates on Metals as a Form of Nanotechnology, Chem. Rev. 105 (2005) 1103–1170. https://doi.org/10.1021/cr0300789.

[3] A.L. Eckermann, D.J. Feld, J.A. Shaw, T.J. Meade, Electrochemistry of redox-active self-assembled monolayers, Coord. Chem. Rev. 254 (2010) 1769–1802. https://doi.org/10.1016/j.ccr.2009.12.023.

[4] A.J. Bard, L.R. Faulkner, Electrochemical Methods: Fundamentals and Applications, 2nd Edition, John Wiley & Sons, New York, 2001.

[5] E. Laviron, Adsorption, autoinhibition and autocatalysis in polarography and in linear potential sweep voltammetry, J. Electroanal. Chem. Interfacial Electrochem. 52 (1974) 355–393. https://doi.org/10.1016/S0022-0728(74)80448-1.

[6] J. Gonzalez, J.A. Sequí-Castellano, Electrochemical determination of kinetic parameters of surface confined redox probes in presence of intermolecular interactions by means of Cyclic Voltammetry. Application to TEMPO monolayers in gold and platinum electrodes, Electrochimica Acta. 365 (2021) 137331. https://doi.org/10.1016/j.electacta.2020.137331.

[7] J. Waelder, S. Maldonado, Beyond the Laviron Method: A New Mathematical Treatment for Analyzing the Faradaic Current in Reversible, Quasi-Reversible, and Irreversible Cyclic Voltammetry of Adsorbed Redox Species, Anal. Chem. 93 (2021) 12672–12681. https://doi.org/10.1021/acs.analchem.1c02503.

[8] T.M. Nahir, E.F. Bowden, The distribution of standard rate constants for electron transfer between thiol-modified gold electrodes and adsorbed cytochrome c, J. Electroanal. Chem. 410 (1996) 9–13. https://doi.org/10.1016/0022-0728(96)04551-2.

[9] J.H. Reeves, Shihua. Song, E.F. Bowden, Application of square wave voltammetry to strongly adsorbed quasireversible redox molecules, Anal. Chem. 65 (1993) 683–688. https://doi.org/10.1021/ac00054a006.

[10] V. Mirčeski, M. Lovrić, R. Gulaboski, Theoretical and experimental study of the surface redox reaction involving interactions between the adsorbed particles under conditions of square-wave voltammetry, J. Electroanal. Chem. 515 (2001) 91–100. https://doi.org/10.1016/S0022-0728(01)00609-X.

[11] J. Gonzalez, J.-A. Sequí, Square Wave Voltcoulommetry Analysis of the Influence of the Electrostatic Environment on the Electrochemical Functionality of Redox Monolayers, ChemElectroChem. 6 (2019) 2290–2301. https://doi.org/10.1002/celc.201900352.

[12] M.S. Ravenscroft, H.O. Finklea, Kinetics of electron transfer to attached redox centers on gold electrodes in nonaqueous electrolytes, J. Phys. Chem. 98 (1994) 3843–3850. https://doi.org/10.1021/j100065a047.

[13] J. Gonzalez, J.-A. Sequí, Kinetic Implications of the Presence of Intermolecular Interactions in the Response of Binary Self-Assembled Electroactive Monolayers, ACS Omega. 3 (2018) 1276–1292. https://doi.org/10.1021/acsomega.7b01995.

[14] S.E. Creager, T.T. Wooster, A New Way of Using ac Voltammetry To Study Redox Kinetics in Electroactive Monolayers, Anal. Chem. 70 (1998) 4257–4263. https://doi.org/10.1021/ac980482l.

[15] E. Laviron, A.C. polarography and faradaic impedance of strongly adsorbed electroactive species: Part I. Theoretical and experimental study of a quasi-reversible reaction in the case of a Langmuir isotherm, J. Electroanal. Chem. Interfacial Electrochem. 97 (1979) 135–149. https://doi.org/10.1016/S0022-0728(79)80057-1.

[16] E. Laviron, A.C. polarography and faradaic impedance of strongly adsorbed electroactive species: Part II. Theoretical study of a quasi-reversible reaction in the case of a Frumkin isotherm, J. Electroanal. Chem. Interfacial Electrochem. 105 (1979) 25–34. https://doi.org/10.1016/S0022-0728(79)80336-8.

[17] E. Laviron, A.C. Polarography and faradaic impedance of strongly adsorbed electroactive species: Part III. Theoretical complex plane analysis for a surface redox reaction, J. Electroanal. Chem. Interfacial Electrochem. 105 (1979) 35–42. https://doi.org/10.1016/S0022-0728(79)80337-X.

[18] S. Guo, J. Zhang, D.M. Elton, A.M. Bond, Fourier Transform Large-Amplitude Alternating Current Cyclic Voltammetry of Surface-Bound Azurin, Anal. Chem. 76 (2004) 166–177. https://doi.org/10.1021/ac034901c.

[19] A.M. Bond, N.W. Duffy, S.-X. Guo, J. Zhang, D. Elton, Changing the Look of Voltammetry, Anal. Chem. 77 (2005) 186 A-195 A. https://doi.org/10.1021/ac053370k.

[20] C.G. Bell, C.A. Anastassiou, D. O'Hare, K.H. Parker, J.H. Siggers, Theoretical treatment of high-frequency, large-amplitude ac voltammetry applied to ideal surface-confined redox systems, Electrochimica Acta. 64 (2012) 71–80. https://doi.org/10.1016/j.electacta.2011.12.088.

[21] E. Laborda, Theoretical-experimental synergy towards better understanding of interfacial electron transfer kinetics, Curr. Opin. Electrochem. 34 (2022) 101028. https://doi.org/10.1016/j.coelec.2022.101028.

[22] J.J. Calvente, R. Andreu, Intermolecular interactions in electroactive thiol monolayers probed by linear scan voltammetry, Curr. Opin. Electrochem. 1 (2017) 22–26. https://doi.org/10.1016/j.coelec.2016.12.006.
[23] E. Laviron, General expression of the linear potential sweep voltammogram in the case of diffusionless electrochemical systems, J. Electroanal. Chem. Interfacial Electrochem. 101 (1979) 19–28. https://doi.org/10.1016/S0022-0728(79)80075-3.
[24] O. Alévêque, E. Levillain, Y. Morille, Alternative voltammetry on self-assembled monolayers: An original approach to estimate the electrochemical electron-transfer rate constants when electroactive adsorbed species interact, J. Electroanal. Chem. 873 (2020) 114414. https://doi.org/10.1016/j.jelechem.2020.114414.
[25] O. Alévêque, P.-Y. Blanchard, C. Gautier, M. Dias, T. Breton, E. Levillain, Electroactive self-assembled monolayers: Laviron's interaction model extended to non-random distribution of redox centers, Electrochem. Commun. 12 (2010) 1462–1466. https://doi.org/10.1016/j.elecom.2010.07.039.
[26] O. Alévêque, E. Levillain, Electroactive mixed self-assembled monolayers: Lateral interactions model updated to interactions between redox and non-redox species, Electrochem. Commun. 34 (2013) 165–169. https://doi.org/10.1016/j.elecom.2013.06.009.
[27] O. Aleveque, F. Seladji, C. Gautier, M. Dias, T. Breton, E. Levillain, Nitroxyl Radical Self-Assembled Monolayers on Gold: Versatile Electroactive Centers in Aqueous and Organic Media, Chemphyschem. 10 (2009) 2401–2404. https://doi.org/10.1002/cphc.200900448.
[28] M.J. Honeychurch, A.M. Bond, Numerical simulation of Fourier transform alternating current linear sweep voltammetry of surface bound molecules, J. Electroanal. Chem. 529 (2002) 3–11. https://doi.org/10.1016/S0022-0728(02)00907-5.
[29] O. Alévêque, P.-Y. Blanchard, E. Levillain, Nitroxyl radical self-assembled monolayers: Generalized lateral interactions model used with binary electrolyte mixture, Electrochem. Commun. 28 (2013) 122–126. http://dx.doi.org/10.1016/j.elecom.2012.12.018.
[30] O. Alévêque, E. Levillain, A generalized lateral interactions function to fit voltammetric peaks of self-assembled monolayers, Electrochem. Commun. 67 (2016) 73–79. https://doi.org/10.1016/j.elecom.2016.04.003.
[31] J.-A. Serret, Cours d'algèbre supérieure : professé à la Faculté des sciences de Paris, Mallet-Bachelier, Paris, France, 1854.
[32] O. Aleveque, P.Y. Blanchard, T. Breton, M. Dias, C. Gautier, E. Levillain, F. Seladji, Nitroxyl radical self-assembled monolayers on gold: Experimental data vs. Laviron's interaction model, Electrochem. Commun. 11 (2009) 1776–1780. https://doi.org/10.1016/j.elecom.2009.07.015.